Experimental and numerical investigations of lattice structures

Liviu Marsavina, Mihai Petru Marghitas, Cosmin Marsavina
University Politehnica Timisoara, Romania
liviu.marsavina@upt.ro, http://orcid.org/0000-0002-5924-0821
miketryiu@yahoo.com, http://orcid.org/0000-0002-4435-2310
cosmin.marsavina@upt.ro, http://orcid.org/ 0009-0004-0648-8155

Davide D'Andrea, Dario Santonocito, Giacomo Risitano
University of Messina, Italy
davide.dandrea@studenti.unime.it, http://orcid.org/0009-0007-1555-4670
dsantonocito@unime.it, http://orcid.org/0000-0002-9709-9638
grisitano@unime.it, http://orcid.org/0000-0002-0506-8720

ABSTRACT. The present work investigates the compressive mechanical response of three lattice structures manufactured via VAT photopolymerization. A bio-inspired architecture, derived from the observation of Euplectella aspergillum, was compared with square and triangular lattice configurations. Experimental uniaxial compression tests and multi-step nonlinear finite element analyses were carried out for each topology to highlight differences in their mechanical behaviour.
The results demonstrate that the bio-inspired structure exhibits superior mechanical performance compared to conventional square and triangular geometries. Furthermore, the proposed simulation methodology proved effective for design purposes, enabling the consideration of instability phenomena and contributing to safer structural design. Finally, micromechanical modelling was employed to link the micro-architecture to the effective macroscopic properties. In particular, a micro-mechanical model allowed to predict the elastic moduli and yield strength, highlighting a stretch-dominated behaviour in elastic regime.

KEYWORDS. Lattice, Bio-inspired, Buckling, micro-mechanical, VAT, Photopolymerization.

OPEN ACCESS

Citation: Marsavina, L., Marghitas, MP., Marsavina, C., D'Andrea, D., Santonocito, D., Risitano G., Experimental and numerical investigations of lattice structures, Fracture and Structural Integrity, 77 (2026) 107-119.

Received: 05.04.2026
Accepted: 15.04.2026
Published: 17.04.2026
Issue: 07.2026

INTRODUCTION

Additive manufacturing (AM) enables the fabrication of finite components directly from a CAD model. This capability has opened new possibilities in mechanical design, as enhanced mechanical properties can be achieved through a tailored spatial distribution of material. Lattice structures consist of assemblies of unit cells arranged in space to optimize material usage by reducing overall volume while maintaining and enhancing certain structural performance.

Numerous studies have focused on enhancing specific component characteristics through modifications of the unit cell architecture, as the geometry of the lattice plays a key role in governing stiffness, strength, deformation mechanisms, and energy absorption behaviour. By tailoring parameters such as cell topology, strut orientation, and relative density, it is possible to optimize the mechanical response of lattice structures for targeted applications. The complexity of these geometries leads researchers to investigate the mechanical behaviour of unit cells and to correlate it to the entire finite part by different approaches. Valvano [1] investigated three cell configurations and derived equivalent mechanical set through homogenisation procedure in order to facilitate tailoring of design parameters.

Unit cell geometries are usually derived from what already exists: They can be inspired from how atoms are arranged in solid materials [1], atomic and molecular orbitals as those proposed by Nuhu et al. [2] and they can emulate organic tissues behavior [3].

Particular attention has been devoted to bio-inspired lattice structures, which are derived from the replication of geometrical patterns and hierarchical features observed in natural systems, such as honeycombs, trabecular bone, bamboo, and cellular plant tissues [4]. These natural architectures have evolved to efficiently balance mechanical performance and material usage, providing high strength-to-weight ratios and enhanced damage tolerance. However, the complexity of resulting stress fields obliges designers to deeply analyse their behaviour. Due to their lightweight nature, high specific stiffness, and large energy absorption capabilities under impact or compressive loading, bio-inspired lattice structures are increasingly adopted in engineering applications. Typical examples include automotive components for crashworthiness and vibration damping, personal protection equipment such as helmets and protective pads [5,6].

In this study, three bio-inspired lattice structures were analysed and experimentally tested. Two architectures were schematized into square and triangular unit cells [7]. The third architecture was inspired by Euplectella aspergillum (E. a.), a deep-sea sponge known for its remarkable energy absorption capability [8].

E. a. typically measures between 6 and 32 cm in length and 1.5–5 cm in diameter. The organism exhibits a predominantly cylindrical morphology that slightly flares toward the upper region, giving it the appearance of a delicate vase or basket. Its structural framework consists of an intricate, grid-like lattice formed by interlocking siliceous spicules that collectively constitute the skeletal system. This lattice architecture is further reinforced by diagonal struts and an external helical ridge oriented perpendicular to the cylindrical surface and spirally wrapped around the body [9].

The mechanical performance of the natural architecture of E. a. was investigated under uniaxial compression by Brown et al. [10]. In their study, both a natural 3×3 unit-cell specimen and a three-dimensionally printed replica, obtained through 3D scanning of the natural structure, were tested in compression, enabling a direct comparison between the native biological architecture and its additively manufactured counterpart. Authors evidenced the complexity of this structure's behaviour but suggested how its characteristics could be used for design purposes if simplified.

A schematic representation of the natural topology was subsequently proposed and analysed by Sharma et al. [8], who caught Brown et al. advice. In this work, the authors simplified the geometry by reinforcing a square lattice with diagonal elements to mimic the load-bearing features of the biological structure. The specimens were manufactured using the FDM process in thermoplastic polyurethane (TPU), as the primary objective of the experimental campaign was to highlight the mechanical response and deformation mechanisms based on local buckling and consequent bending of the bio-inspired unit cell. The capability of this material, which was modelled as hyperelastic due to the extreme strains it can sustain before failure, evidenced the potential of this architecture for energy absorption applications.

Two-dimensional (2D) and three-dimensional (3D) lattice structures can be designed to achieve either isotropic or anisotropic behaviour, depending on the required mechanical performance. Moreover, it is possible to tailor specific mechanical characteristics in selected regions of a component by employing graded lattice structures, in which geometric parameters such as cell size, strut thickness, or topology vary spatially due to load condition they are subjected to [11].

While numerous studies have investigated similar geometries fabricated from steels and polymers using powder bed fusion–based processes, such as Selective Laser Melting (SLM), Electron Beam Melting (EBM), Selective Laser Sintering (SLS), Multijet Fusion, and Fused Deposition Modelling, the literature lacks comprehensive investigations into the mechanical

behaviour of such structures manufactured via photopolymerization (vat) processes, which allows to obtain fine quality and high resistance.

The photopolymerization process uses liquid resins and photopolymers as its primary materials and consists of triggering chemical reactions through irradiation with ultraviolet or visible light, leading to solidification [12]. These include layer thickness, build orientation and printing velocity for all technologies; laser energy for SLS and SLM; nozzle and bed temperature for FDM; and part positioning within the printing chamber for the MJF process [13–15]. For vat photopolymerization technologies, the main process parameters consist of exposure time, light intensity, layer thickness, build orientation, and resin-related properties, all of which significantly influence the final mechanical and physical characteristics of the printed parts [16].

Vat photopolymerization can be divided into two main variants: stereolithography (SLA), which solidifies liquid resin using a moving energy source, and digital light processing (DLP), which cures an entire layer in a single exposure. Both technologies are characterized by high processing speed and are well suited for rapid prototyping applications, offering very high resolution and enabling multi-material additive manufacturing. On the other hand, they require post-processing steps, demand skilled operators, and involve the handling and disposal of liquid resins, which are toxic and require careful management [17].

Experimental observations obtained from uniaxial compression tests performed on the three proposed lattice structures highlighted that buckling is a dominant phenomenon governing their mechanical response. FEM simulations were carried out to determine the critical displacement associated with the onset of buckling. The post-buckling behaviour of the structures was then evaluated by introducing the corresponding buckled deformed shape of each layout as an initial geometric imperfection in subsequent nonlinear analyses [18]. A similar approach was also proposed by Śledziewski and Górecki [19], by employing the RIKS analysis available in Abaqus, which allows to investigate through the bifurcation point in force convergence.

Moreover, lattice structures can be effectively described through micromechanical models that relate their micro-architecture to the resulting macroscopic mechanical properties. According to the Gibson–Ashby theory [20,21], the effective properties of cellular materials are dependent on relative density through power-law relationships, where the scaling exponent depends on the dominant deformation mechanism within the cell walls. These micromechanical models provide a methodology for predicting stiffness and strength of lattice structures based on their geometry and relative density. The micromechanical approaches to evaluate the mechanical properties of cellular structure were employed successful for polymeric [16] and aluminium foams [17].

In this paper experimental compressive tests are performed on three lattice structures obtained via Vat photopolymerization and their mechanical behaviour is simulated via FE analysis considering compressive loads and buckling analysis. FE analysis was carried out using a multi-step approach and employing an isotropic elastic material model. Few works focused on FEM simulations of mechanical behaviour of parts manufactured by resin-process. Lovo et al. [22] stated that it is possible to approximate the resin as an isotropic linear material due to the high geometric quality which can be obtained from photopolymerization process and post processing. Moreover, based on authors experience, using an isotropic material for vat resin gave results coherent with experimental fracture mechanic tests [23].

First, a nonlinear analysis was conducted to determine the displacement at which buckling occurs. The resulting deformed configuration was then introduced as an initial geometric imperfection in a subsequent analysis to evidence post-buckling behavior. By doing so, it was possible to focus on specimen-specific imperfections, which cannot be captured when using a simple isotropic material model. Finally, mechanical properties are discussed and predicted adopting micro-mechanical modelling.

EXPERIMENTAL EVALUATION

Materials and specimen manufacturing

Lattice structures were designed with CAD software SolidWorks adopting three elementary cells (Fig. 1): square, triangle and bio-inspired by deep sea sponge Euplectella aspergillum (E. a.) [18].

The Digital Light Processing manufacturing technique was employed to produce the specimens, with a commercial ANYCUBIC Photon – LCD printer. The main characteristics of the printer are: a LED UV, 405 nm, 25 W light source, a building volume of 115 x 65 x 155 mm, a XY resolution 2560×1440 pixels, 47 μm, with minimum layer thickness between 0.01 to 0.2 mm, a printing speed of 20 mm/h and using a 405nm UV Resin, commercially named Translucent Green. Considering our experience on the influence of manufacturing parameters on tensile [17] and fracture toughness [16], the manufacturing parameters employed for fabrication of the lattice structures are presented in Tab. 1, where an in-plane

printing with 0.05 mm layer thickness and an exposure time of 3.6 seconds for each layer were adopted. The post processing procedure was performed by cleaning in Isopropyl Alcohol (IPA) for 5 minutes and curing for 5 minutes with UV radiation. For each lattice structure four specimens were manufactured.

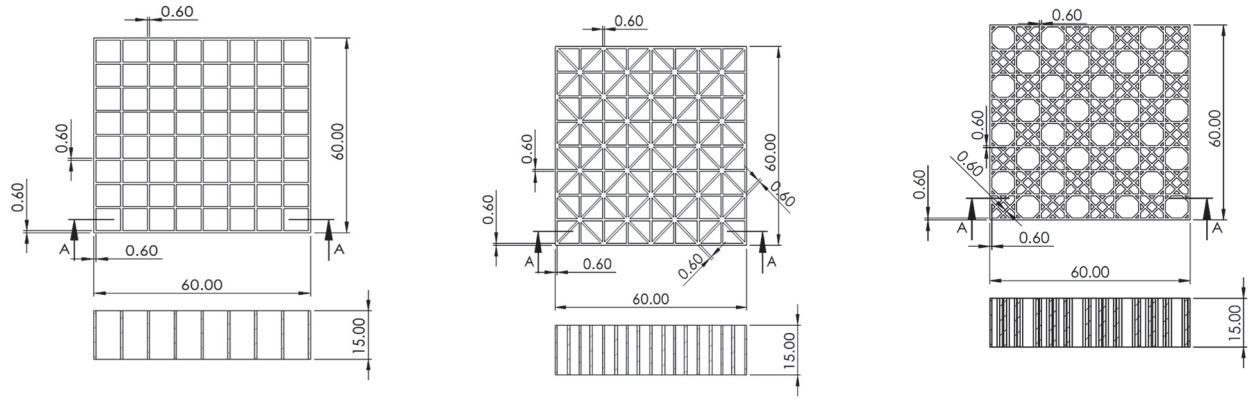

Figure 1: Lattice structures dimensions expressed in millimeters for: a) square-lattice; b) triangular-lattice; c) Euplectella Aspergillum inspired.

Specimen orientation	Layer thickness [mm]	Exposure time [s]	Cleaning time [min]	Curing time [min]
In plane	0.05	3.6	5 (in IPA)	5 (UV)

Table 1: Manufacturing process parameters.

After curing, all the specimens were weighted to determine the mass ($m_{lattice}$). The lattice structures densities were determined ($\rho_{lattice}=m_{lattice}/V_{lattice}$), with $V_{lattice}$ the volume of the lattice structure, resulted from the CAD model. The material density was determined by printing with the same manufacturing parameters some cubes of 10 mm edge, which were also weighted, to obtain the solid density ($\rho_{solid}=m_{solid}/V_{solid}$). Then, the relative densities of the lattice structures were determined as $\rho_{lattice}/\rho_{solid}$.

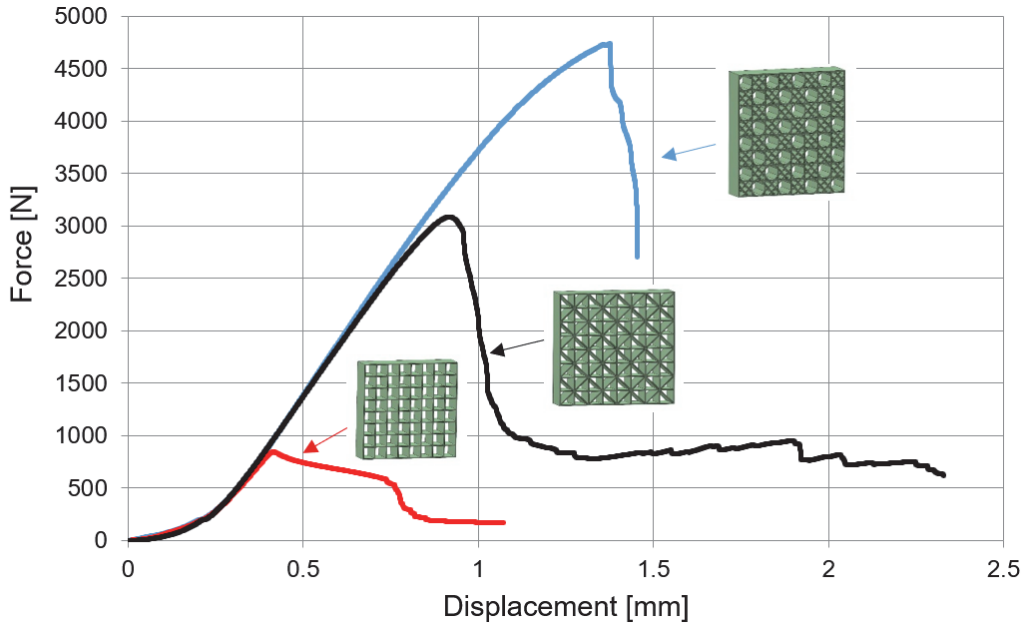

Figure 2: Load-displacements curves for the considered lattice structures.

Compression tests

The compression tests of lattice structures were performed with 5 mm/min displacement control, at room temperature (23 °C) using a Zwick ProLine Z005 testing machine. A digital camera was used to record the test and analyse the deformation behaviour of the lattice structures. Typical load-displacement curves for one specimen are shown in Fig. 2 for the three lattice structure considered.

The E.a. inspired lattice structure exhibits the maximum value of compressive force, followed by the triangle honeycomb and, finally, by the square lattice. The resulted failures of the lattice structures under compression are different (Fig. 3). The square lattice exhibits an elastic buckling followed by the faces bend and tensile before fracture (Fig. 3a). For the triangle lattice, a local buckling occurs at the edge of the structure and then the struts of the structure failed due to a combination of tensile and bending (Fig. 3b). The E.a. inspired structure mitigated pronounced buckling or local buckling phenomena. The fracture occurred at 45° through the structure by shear.

The measurements of the specimen's mass and dimensions, and maximum load are presented in Tab. 2.

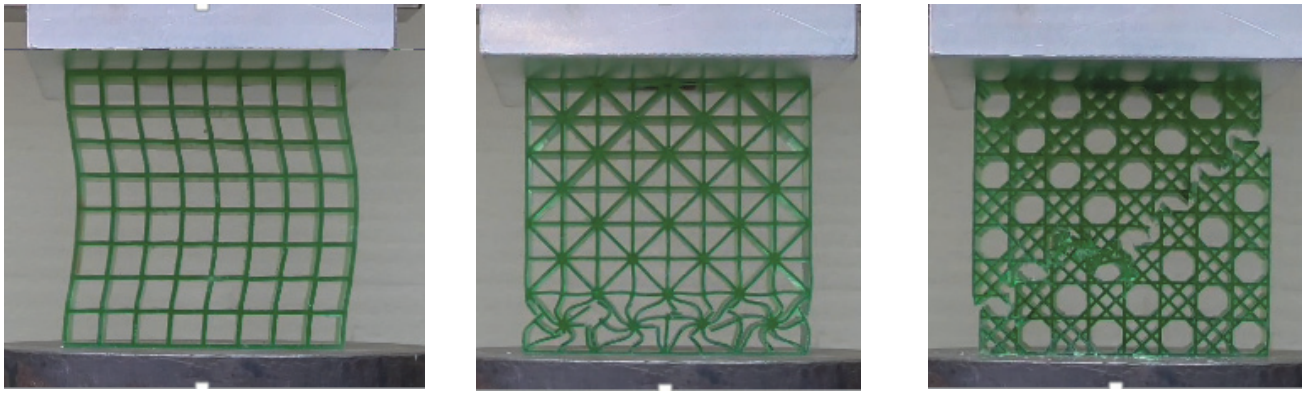

(a) (b) (c)

Figure 3: Failures frame for a) square-lattice; b) triangular-lattice; c) E.a. inspired structure.

Specimen Number.	Weight, m [g]	Specimen dimensions (L_1xL_2xt) L_1 [mm]	L_2 [mm]	t [mm]	Density $\rho_{lattice}$ [g/cm^3]	Maximum load F_{max} [N]
			Square-lattice			
P1	13.447	59.80	59.80	15.10	0.249	801
P2	12.902	59.70	59.75	15.05	0.240	844
P3	13.263	59.75	59.70	15.05	0.247	1050
P4	13.257	59.75	59.70	15.00	0.248	1060
			Triangular-lattice			
T1	20.865	59.80	59.80	15.15	0.385	2720
T2	20.864	59.80	59.80	15.05	0.388	2980
T3	20.505	59.75	59.80	15.05	0.381	3090
T4	20.767	59.80	59.80	15.05	0.386	3130
			Euplectella Aspergillum inspired			
C1	25.701	59.70	59.75	15.15	0.476	4990
C2	25.708	59.75	59.70	15.16	0.475	4760
C3	26.68	59.75	59.73	15.15	0.493	5060
C4	25.996	59.80	59.80	15.17	0.479	4740

Table 2: Specimens dimensions and maximum load.

NUMERICAL SIMULATION

Preprocessing and workflow explanation

Finite element model analyses were carried out to investigate each structure's behaviour in compression tests. To do this, non-linear static structural analysis has been implemented in Ansys Workbench 2025 r2 environment. To correctly describe stress and strain fields and to limit the number of elements, these structures were schematized by 2D plain strain condition, since the thickness dimension is comparable to the height and width and the work focuses only on in-plane mechanical behavior [24]. Vat resin was modelled as isotropic elastic material characterized by Young's Modulus equal to 1300 MPa and Poisson Ratio equal to 0.38. A very fine free quadrilateral mesh with an element size of 0.15 mm was employed, as determined through a mesh sensitivity analysis which was conducted to identify the element size that provides a total strain energy for each configuration comparable to those obtained with a much finer mesh of 0.01 mm, which would have been computationally prohibitive for a multistep nonlinear analysis. Results in term of percentage differences are reported in Fig. 4a.

The selected mesh ensured at least four elements along the thin vertical and horizontal walls, as well as along the diagonal struts [25]. To avoid any singularity depending on boundary conditions, displacements were given to compression plates, simplified as rigid elements. The contacts were set to be "frictional" with a friction coefficient of 0.2. A multistep analysis was set in order to investigate multiple points in the force-displacement curve. Additionally, large displacement's option was activated to determine if the deformed shape modifies its stiffness accordingly to the onset of large deformations. Contacts and large displacements cause the analysis to be non-linear and, to ensure convergence in results, each step is characterized by an increase in negative vertical direction of 0.05 mm. Fig. 4b-d illustrates the layouts adopted for the FEM analysis. The compression plates, shown in blue, are simplified as rigid bodies, whereas the lattice structures, depicted in green, are modelled as isotropic elastic materials, as previously described. The interfaces between the compression plates and the lattice structures are defined as frictional contact surfaces to prevent interpenetration between components while allowing sliding and separation resulting from structural deformation.

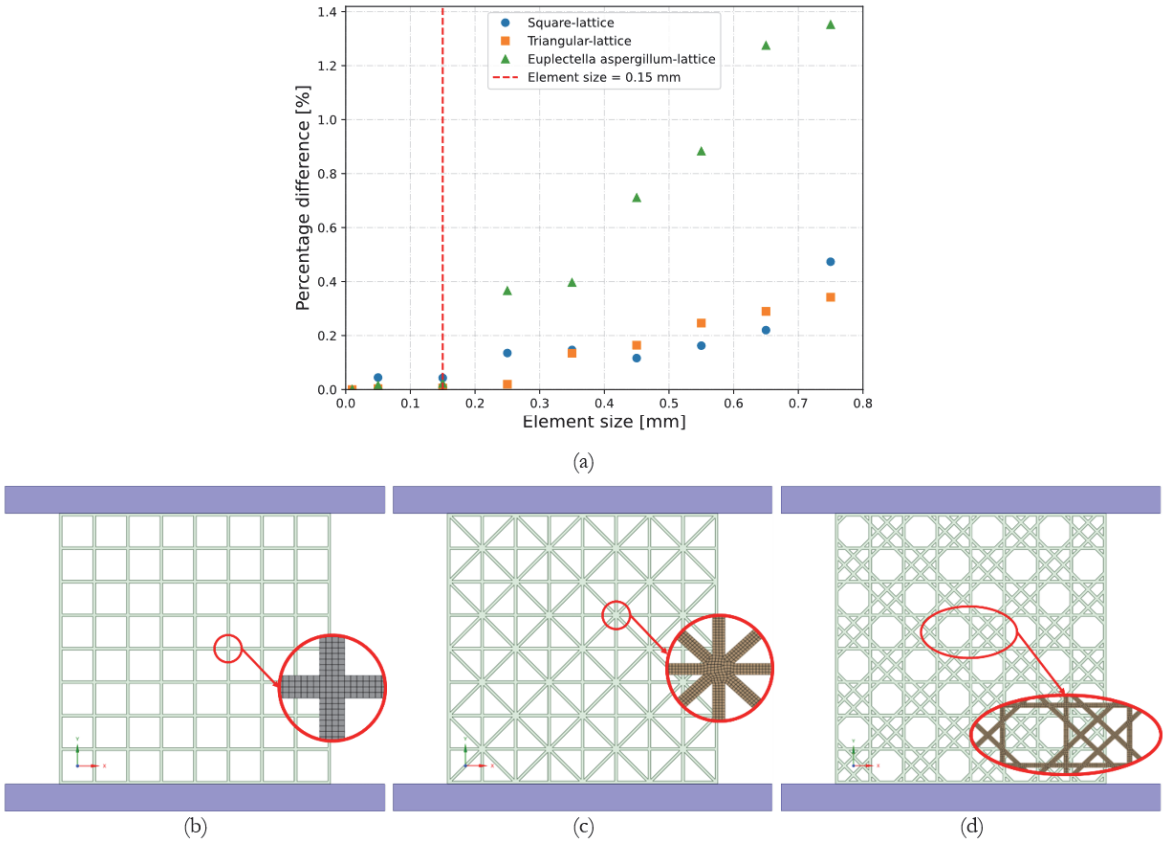

Figure 4: a) Mesh sensitivity analysis results; b)Square; c)Triangular; d)Euplectella aspergillum lattice structures geometries and mesh details.

Since buckling was observed in both square and triangular lattice structures, a non-linear eigenvalue buckling analysis was performed in each geometry. Buckling analysis gives the buckling deformed shape and the load multiplier which, if multiplied to the applied force, gives the critical force depending on material and structure's layout stiffness. Because the applied boundary conditions consisted in displacement and not in a force, each load-step was used as a basis for buckling analysis, in order to find out which displacement condition corresponded to a load multiplier tending to one: in this condition the applied displacement corresponds to the critical load in compression.
The resulting deformed shape corresponding to the first buckling mode was extracted as STL file and repaired in Spaceclaim environment to be converted in surface again. An explicative workflow chart is reporter in Fig. 5, in which it is possible to observe the boundary conditions consisting in a multistep rigid "remote displacement", pointed out as u_y (coherent with the experimental displacements measured in correspondence of the maximum load) assigned to the upper compression plate, and a fixed remote displacement in the lower plate. The lattice structure is represented as a general one since the boundary conditions were the same for each layout investigated in this work. Each stress field obtained by each load step was used as a pre-stress pattern for non-linear eigenvalue buckling analysis in order to determine the load step corresponding to a displacement leading to the critical load. Finally, the deformed shape associated with critical load is extracted as STL mesh and repaired as a surface to be analysed with a static structural analysis.

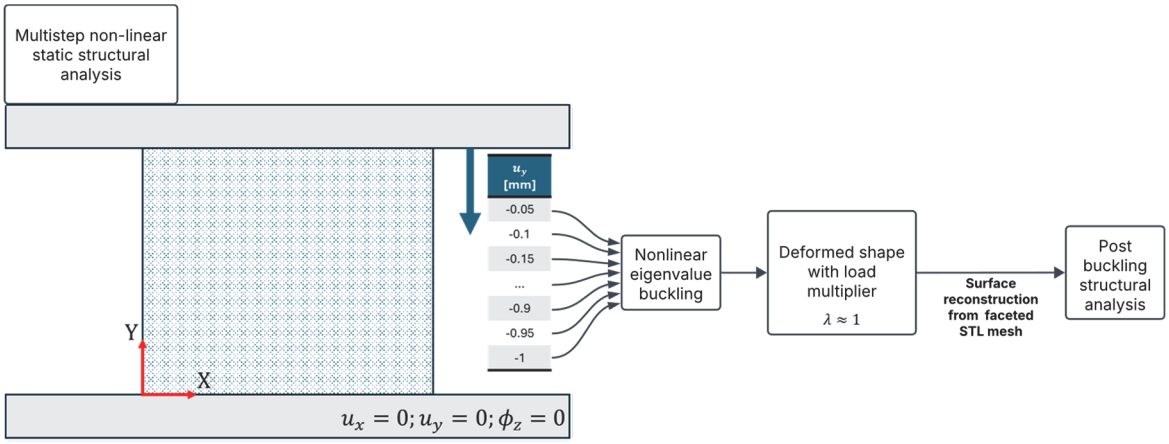

Figure 5: FEM analysis' workflow.

This process allowed to investigate structures post-buckling behaviour, since it was experimentally observed that after the occurrence of buckling the sample continued to resist. This is due to the fact that these lattice structures are designed for energy absorption applications and are commonly manufactured with materials which can be modelled as hyperelastic. While the lattice structures shape can be characterized by large strain energy, vat resin shows a quasi-brittle behaviour with ultimate stress almost coincident with the yield stress according to ASTM D638 standard.

Results

Eigenvalue nonlinear buckling analysis made it possible to determine the maximum displacement that each VAT-resin-manufactured structure could withstand before the onset of local buckling. However, this condition does not necessarily correspond to the failure of the lattice sample, as experimental observations showed that the structure is still able to sustain load even after transitioning into its buckled configuration. Tab. 3 reports critical displacements estimated by FEM analysis for each configuration. Results are coherent with experimental results, since it was observed how for the square-lattice configuration, due to its slenderness, buckling occurred almost immediately after contact began, suggesting that the critical displacement of 0.1 mm is in line with experimental observation. A substantial increase in critical displacement was estimated for the triangle lattice structure, which resulted to be equal to 0.35 mm. Although local buckling was not observed in uniaxial compressive tests performed on the lattice structure inspired by E.a., since failure occurred in a brittle manner along one of the diagonals, a critical displacement of 1.25 mm was estimated through FEM analysis.
This discrepancy can be attributed to manufacturing-induced defects and to deviations from the nominal geometry resulting from the dimensional tolerances of the AM manufactured specimen. Additionally, the deformed shape consequent buckling consists in localized strain in the interface between the sample and the compression plate.
In addition to what was discussed before, each structure stiffness was calculated as the ratio between the frictional contact vertical reaction force and the displacement applied. By doing so, it was possible to observe how the structure characterized

by the lowest stiffness is the square-lattice. If it is taken as a reference, triangular-lattice shows an increase in stiffness of 25.6%, while the E.a. inspired lattice structure an increase of 37.6%. The same considerations can be extended to the critical load: the triangular-lattice exhibits a critical load 3.3 times higher than that of the square layout, while the E.A.-inspired structure is characterized by a critical load 15.3 times greater than the square-lattice.

Lattice structure	Stiffness K [N/mm]	Critical displacement [mm]	Load Multiplier [//]	Critical Load [N]
Square-lattice	2068.2	0.1	0.98	208
Triangular-lattice	2597.8	0.35	1.02	903
Euplectella Aspergillum-inspired	2846.4	1.25	1.07	3394

Table 3: FEM results.

Fig. 6 presents the buckled configurations for each lattice structure. The FEM-predicted deformed shape of the square lattice agrees well with the experimentally observed configuration. In contrast, the triangular lattice exhibits a deformation pattern distributed along the entire left side in the first buckling mode. Conversely, the E.a.-lattice structure exhibits localized buckling, with deformation primarily concentrated at the corners, although experimental failure occurred along one of the diagonals.

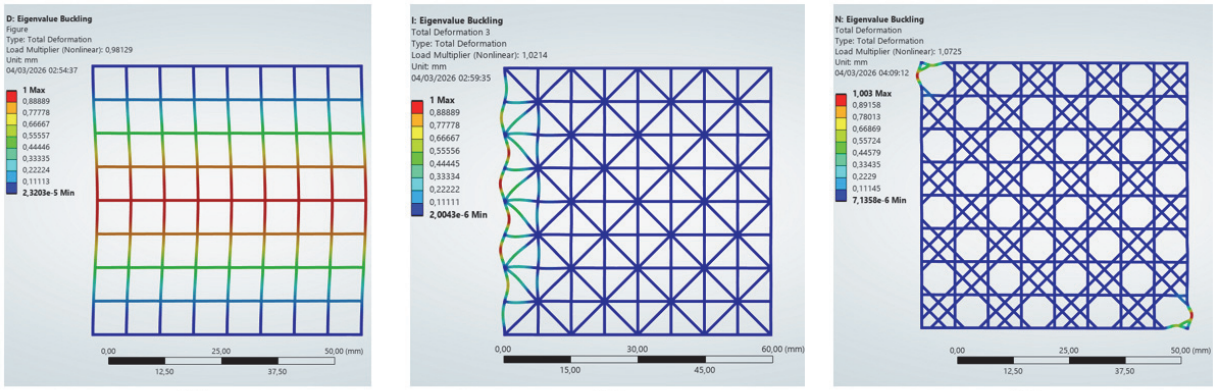

(a) (b) (c)

Figure 6: Buckling deformed shapes for a) square-lattice; b) triangular-lattice; c) E.a. inspired lattice structure.

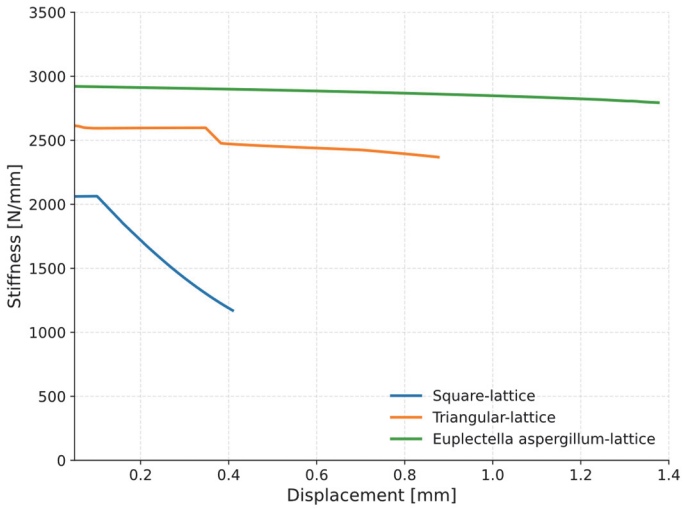

Figure 7: Stiffness variation in post-buckling simulations.

The FE model predicts a critical displacement for the E.a.-inspired structure of 1.25 mm, relatively larger than the ones predicted for the square (0.1 mm) and triangle lattice (0.35 mm). This indicate that buckling would occur only at large

deformation level which, in practice, is never reached by the E.a inspired structure due to the brittle fracture that intervenes first. The E.a inspired architecture suppresses buckling and move the material failure mode from geometric instability to material failure.
Post-buckling analysis made it possible to quantitatively evaluate the change in stiffness, calculated as the ratio between the applied displacement and the calculated reaction force in the lower contact region, associated with the buckled configuration This was achieved by using the deformed shape corresponding to the critical displacement as the initial geometry for a subsequent multi-step nonlinear static structural analysis. Fig. 7 illustrates the stiffness variation for each lattice structure in the buckled state.
It can be observed that, for both the square and triangular lattice structures, an instantaneous deviation from an initially constant stiffness value occurs as a direct consequence of buckling. In contrast, the E.a.-inspired structure exhibits a continuously varying stiffness throughout the entire simulation, without a clearly defined plateau region.
Finally, the reaction force leading the specimens to failure was calculated by FEM model extracting the reaction force value estimated in correspondence of the experimental displacement leading the specimens to failure in the post-buckling analysis.

Comparison with experimental tests

It is possible to compare the results coming from the experimental compressive tests with the prediction of the FE simulations of compression failure and buckling. In Fig. 8, for each lattice structure, the diamonds represent the average value of experimental compression failure force, calculated by the points represented by circles and followed by error bars representing the standard deviation of the samples in force and relative density on four specimens. The "x" marker points indicate the failure load estimated by FE models, extracted in correspondence of experimental failure displacements; finally, the squares represent the critical forces causing buckling estimated by non-linear eigenvalues buckling analysis.

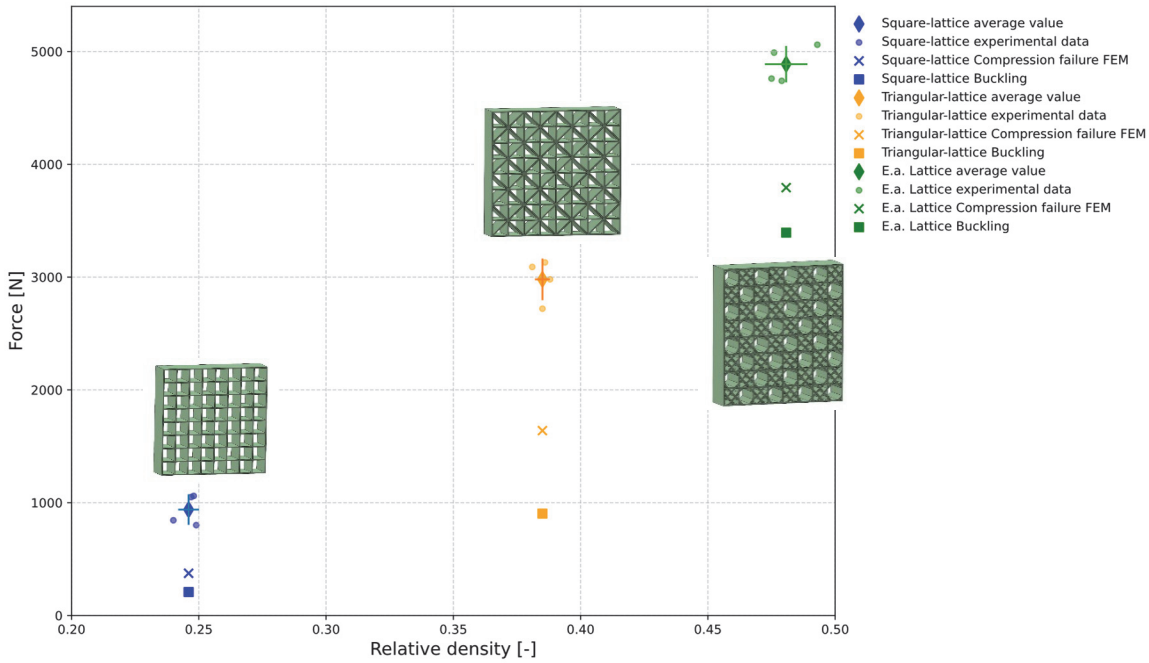

Figure 8: Comparison of experimental test with FE simulations.

For the square-lattice, the experimental failure has higher value (938±135 N) compared to the compression (374 N) and buckling (208 N) loads estimated by FEM. The difference is more marked considering the triangular-lattice and E.a. inspired structure; indeed, the first has a failure load of 2980±184 N, a compression load of 1639 N and a buckling load of 903 MPa, while the latter has a failure load of 4887±161 N, a compression load of 3793 N and a buckling load of 3394 MPa. The difference between the compression load and the buckling load of the triangle lattice seems more pronounced since the buckling phenomenon interest a large part of the sample; on the other hand, in the square lattice and E.a. inspired structure it involves smaller area of the specimens (Fig. 6). Another explanation to the increase in critical displacement, and consequently of critical load, is that each structure's unit cell can be seen as a square unit cell reinforced with diagonals struts, and these reinforcements influence both critical and fracture load. The under estimation of experimental failure loads

by FE models can be attributed to a combination of modelling assumptions. The 2D plane strain simplification constrains out-of-plane deformation, preventing the stress redistribution that occurs in real specimens during post-buckling, especially in the triangular lattice and E.a. inspired geometry, where internal stress paths are more complex. The isotropic linear elastic material model, already adopted for Vat photopolymerized resins, cannot capture the post yielding stress redistribution nor the continued load-bearing capacity experimentally observed after the onset of local buckling. Finally, the FE model does not account for the local increase in cross-sectional area at strut nodes resulting from the light overcure effect inherent to Vat photopolymerization, which increases the effective stiffness of the real specimens. Despite these limitations, the FE model proves conservative with respect to the experimental failure loads, which represents an acceptable and desirable characteristic for design-oriented simulations.

MICRO-MECHANICAL MODELING

The micromechanical models for cellular structures aim to link the micro-architecture (cell geometry, topology, and material of struts and walls) to the effective macroscopic properties (stiffness, strength, plasticity, fatigue, thermal behaviour) [20]. Below is a structured overview of the main model classes used in research and engineering.
Generally, a micromechanical model can be expressed by:

$$\text{Property}_{\text{lattice}}=C\left(\frac{\varrho_{\text{lattice}}}{\varrho_{\text{solid}}}\right)^{n}\text{Property}_{\text{solid}} \tag{1}$$

where C and n represent fitting parameters.
For linear elastic lattices the behaviour of walls is stretch dominated or bending dominated. Accordingly, the Young's modulus can be estimated:

- for stretch dominated with [20]

$$E_{\text{lattice}}=\left(\frac{\varrho_{\text{lattice}}}{\varrho_{\text{solid}}}\right)E_{\text{solid}} \tag{2}$$

- for bending dominated with [20]

$$E_{\text{lattice}}=\left(\frac{\varrho_{\text{lattice}}}{\varrho_{\text{solid}}}\right)^{2}E_{\text{solid}} \tag{3}$$

The compression strength could be estimated considering plastic collapse of cell edges in bending, [21]:

$$\sigma_{\text{lattice}}=C_{\sigma}\left(\frac{\varrho_{\text{lattice}}}{\varrho_{\text{solid}}}\right)^{3/2}E_{\text{solid}} \tag{4}$$

with C_σ ranging from 0.4 – 1.0.
Fig. 8 presents the micromechanical model for Young's Modulus, where it can be observed from its distribution that for the elastic region the cell walls for all three lattice structures follow a stretching behaviour. In Fig. 9 it can be observed the experimental results versus the micromechanical models to predict the compression strength. At low relative density for square lattice, C_σ=0.4; while increasing the relative density the experimental data fit the micromechanical model corresponding to C_σ=1.0 for triangle and E.a. inspired lattice.

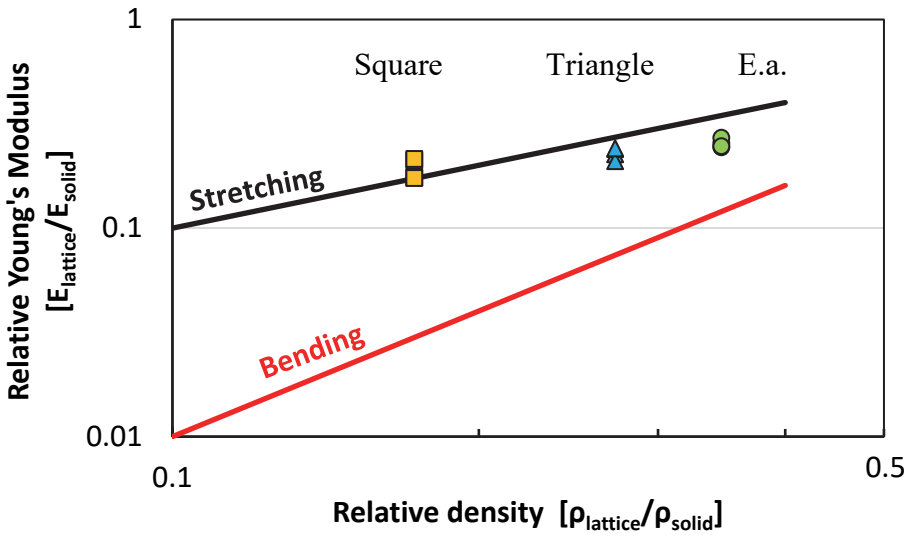

Figure 9: Micromechanical models versus experimental data for Young's Modulus (log-log diagram).

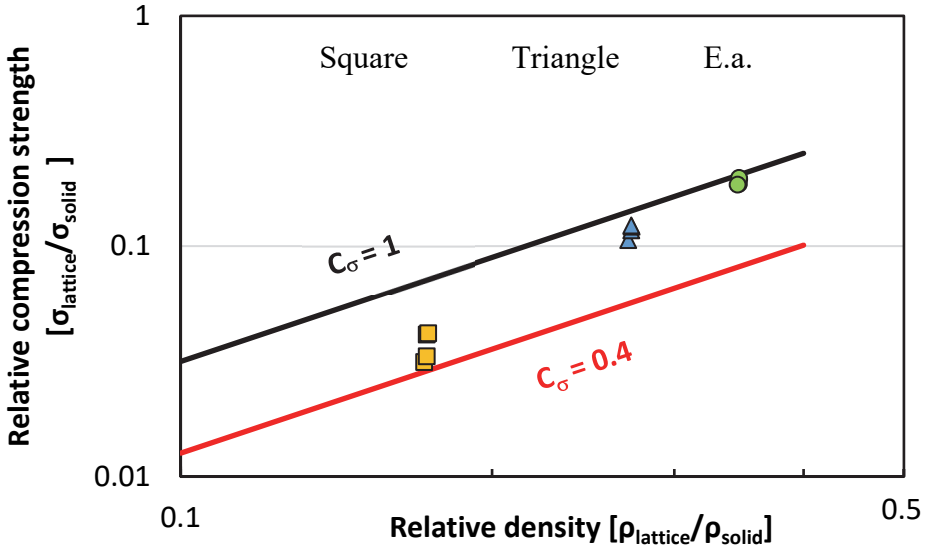

Figure 10: Micromechanical models versus experimental data for compression strength (log-log diagram).

Conclusions

The bio-inspired E.a. structure highlighted the highest load bearing. The square and triangular lattice fail by buckling with, respectively, a global one for the square lattice, a local one for the triangular lattice. The geometry of the bio-inspired structure prevents the occurrence of buckling.

Numerical simulations on each lattice structure geometry have been carried out to investigate specimens' behaviour in both the elastic and post buckling phase. To do this, multistep non-linear FEM analysis was performed to determine the critical displacement leading to buckling, which, once it was determined, was used as a starting point for further analysis on the deformed shape, which allowed authors to investigate changes in stiffness associated with buckling arise. The study highlighted that the stiffness of square and triangle lattice structures is significantly affected by the occurrence of buckling. In contrast, the bio-inspired lattice structure investigated in this study does not exhibit a pronounced reduction in stiffness, instead showing an almost linear decrease. This behaviour is further supported by experimental observations, which did not

reveal any significant buckling occurrence and instead resulted in a brittle failure along one of the lattice diagonals. Moreover, in addition to the critical displacement, the FEM model enabled the estimation of the critical load at which buckling occurs. However, the model did not accurately capture the experimental compressive failure load. The micromechanical modelling represents a useful tool to estimate the mechanical properties of lattice structures.

Further studies will be developed employing local approaches, since the complexity of these structures causes the macroscopical metrics used for comparison inconsistent. The underlying concept of local approaches is that both static and fatigue failure are governed by local stress intensification. Defects, discontinuities, or notches can cause stress fields to reach critical values. In particular, the averaged strain energy density (ASED) provides insight into mechanical behaviour by evaluating the critical strain energy within a defined control area, whose radius is a characteristic of the specific material [26]. While knowledge of the control radius is essential for obtaining quantitative information on failure phenomena, parameters from linear elastic fracture mechanics can be used as reference targets for comparison, with the aim of minimizing ASED.

ACKNOWLEDGEMENTS

This work was supported by a grant of the Ministry of Research, Innovation and Digitization, CNCS-UEFISCDI, project number PN-IV-P1-PCE-2023-1446, within PNCDI IV.

REFERENCES

[1] Valvano, S. (2025). Homogenised properties of lattice metal composite cell. Facta Universitatis, Series: Mechanical Engineering 23, pp. 735–56. DOI: https://doi.org/10.22190/FUME240125015V.

[2] Nuhu, A.A., Elmoghazy, Y.H., Al Mahmoud, Z., Petrů, J., Sahmani, S., Safaei, B. (2026). TPMS-based hyperboloidal primitive architectured structures with a novel hybridization method. Int J Mech Sci 312, 111206. DOI: https://doi.org/10.1016/J.IJMECSCI.2026.111206.

[3] Singh, G., Gupta, V., Chanda, A. (2025). Mechanical characterisation of rotating triangle shaped auxetic skin graft simulants. Facta Universitatis, Series: Mechanical Engineering 23, pp. 79–94. DOI: https://doi.org/10.22190/FUME220226038S.

[4] Greco, L., Buccino, F., Xu, Z,, Vergani, L., Berto, F., Guagliano, M. (2023). Design and Analysis of Energy Absorbent Bioinspired Lattice Structures. Journal of Bionic Engineering 20(4), pp. 1670–1686. DOI: https://doi.org/10.1007/s42235-023-00358-6.

[5] Koech, A.K., Mwandila, G., Mulolani, F. (2026). Crashworthiness performance of bio-inspired BCC lattice structures: Comparative evaluation of aluminum, neat jute epoxy, and hybrid glass/jute epoxy composite structures. Compos Struct 376, 119792. DOI: https://doi.org/10.1016/j.heliyon.2024.e34806.

[6] Chen, Z., Li, J., Wu, B., Chen, X., Ren, X., Xie, Y.M. (2023). A novel bio-inspired helmet with auxetic lattice liners for mitigating traumatic brain injury. Smart Mater Struct32, 105020. DOI: https://doi.org/10.1088/1361-665X/acf62e.

[7] Zhang, Q., Yang, X., Li, P., Huang, G., Feng, S., Shen, C. (2015). Bioinspired engineering of honeycomb structure – Using nature to inspire human innovation. Prog Mater Sci 74, pp. 332–400. DOI: https://doi.org/10.1016/j.pmatsci.2015.05.001.

[8] Sharma, D., Hiremath, S.S. (2022). Bio-inspired repeatable lattice structures for energy absorption: Experimental and finite element study. Compos Struct 283, 115102. DOI: https://doi.org/10.1016/j.compstruct.2021.115102.

[9] Santivongskul, P., Fox, K., Tran P. (2025). Microstructural hierarchy of Euplectella aspergillum: mechanical insights and biomimetic applications. Bioinspir Biomim 20, 051001. DOI: https://doi.org/10.1088/1748-3190/adfb18.

[10] Robson Brown, K., Bacheva, D., Trask, R.S. (2019). The structural efficiency of the sea sponge Euplectella aspergillum skeleton: Bio-inspiration for 3D printed architectures. J R Soc Interface 16. DOI: https://doi.org/10.1098/rsif.2018.0965.

[11] Panesar, A., Abdi, M., Hickman, D., Ashcroft, I. (2018). Strategies for functionally graded lattice structures derived using topology optimisation for Additive Manufacturing. Addit Manuf 19, pp. 81–94. DOI: https://doi.org/10.1016/j.addma.2017.11.008.

[12] Gibson. I., Rosen, D., Stucker, B. (2015). Vat Photopolymerization Processes. Additive Manufacturing Technologies, pp. 63–106. DOI: https://doi.org/10.1007/978-1-4939-2113-3_4.

[13] Gao, G., Xu, F., Xu, J., Tang, G., Liu, Z. (2022). A Survey of the Influence of Process Parameters on Mechanical Properties of Fused Deposition Modeling Parts. Micromachines 13. DOI: https://doi.org/10.3390/mi13040553.
[14] Dzienniak, D. (2022). The Influence of the Material Type and the Placement in the Print Chamber on the Roughness of MJF-Printed 3D Objects. Machines 10. DOI: https://doi.org/10.3390/machines10010049.
[15] Joch, R., Šajgalík, M., Drbúl, M., Měřínska, D., Markovič, J., Czán, (2025). A. Impact of powder bed fusion printing process parameters on the achieved quality of PA12 manufactured parts. Progress in Additive Manufacturing 10(7) pp. 4123–4141. DOI: https://doi.org/10.1007/s40964-025-01053-0.
[16] Brighenti, R., Cosma, M.P., Marsavina, L., Spagnoli, A., Terzano, M. (2020). Laser-based additively manufactured polymers: a review on processes and mechanical models. Journal of Materials Science 56(2), pp. 961–998. DOI: https://doi.org/10.1007/s10853-020-05254-6.
[17] Brighenti, R., Cosma, M.P., Marsavina, L., Spagnoli, A., Terzano, M. (2021). Multiphysics modelling of the mechanical properties in polymers obtained via photo-induced polymerization. The International Journal of Advanced Manufacturing Technology 117(1), pp. 481–499. DOI: https://doi.org/10.1007/s00170-021-07273-2.
[18] Baumgardt, G.R., Fragassa, C., Rocha, L.A.O., dos Santos, E.D., da Silveira, T., Isoldi, L.A. (2023). Computational Model Verification and Validation of Elastoplastic Buckling Due to Combined Loads of Thin Plates. Metals, 13. DOI: https://doi.org/10.3390/met13040731.
[19] Śledziewski, K., Górecki, M. (2020). Finite Element Analysis of the Stability of a Sinusoidal Web in Steel and Composite Steel-Concrete Girders. Materials 13. DOI: https://doi.org/10.3390/ma13051041.
[20] Gibson, L.J., Ashby, M.F. (1997). Cellular Solids: Structure and Properties, Cambridge Solid State Science Series, Cambridge University Press, Cambridge.
[21] Ashby, M.F., Medalist, R.F.M. (1983). The mechanical properties of cellular solids.
[22] Lovo, J.F.P., de Camargo, I.L., Erbereli, R., Morais, M.M., Fortulan, C.A. (2020). Vat Photopolymerization Additive Manufacturing Resins: Analysis and Case Study. Materials Research 23, e20200010. DOI: https://doi.org/10.1590/1980-5373-MR-2020-0010.
[23] Marghitas, M., Popa, C.F., Marsavina, L. (2025). On the Size and Notch Effect in AM Photo-Polymerized Components. Fatigue Fract Eng Mater Struct 48, pp. 3790–3804. DOI: https://doi.org/10.1111/FFE.70001;WGROUP:STRING:PUBLICATION.
[24] Sharma, D., Hiremath, S.S. (2023). Experimental and FEM study on the in-plane and out-plane loaded reversible dual-material bio-inspired lattice structures with improved energy absorption performance. Compos Struct 303, 116353. DOI: https://doi.org/10.1016/J.COMPSTRUCT.2022.116353.
[25] Sharma, D., Hiremath, S.S. (2023). In-plane elastic properties of the Euplectella aspergillum inspired lattice structures: Analytic modelling, finite element modelling and experimental validation. Structures 48, pp. 962–975. DOI: https://doi.org/10.1016/J.ISTRUC.2023.01.002.
[26] du Plessis, A., Razavi, N., Benedetti, M., Murchio, S., Leary, M., Watson, M. (2023). A probabilistic average strain energy density approach to assess the fatigue strength of additively manufactured cellular lattice materials. Int J Fatigue 172, 107601. DOI: https://doi.org/10.1016/j.pmatsci.2021.100918.